

Solution of Advection Equation with Discontinuous Initial and Boundary Conditions via Physics-Informed Neural Networks

Omid Khosravi Mehdi Tatari

Department of Mathematical Sciences, Isfahan University of Technology, Isfahan,
84156-83111, Iran

Abstract

In this paper, we investigate several techniques for modeling the one-dimensional advection equation for a specific class of problems with discontinuous initial and boundary conditions using physics-informed neural networks (PINNs). To mitigate the spectral bias phenomenon, we employ a Fourier feature mapping layer as the input representation, adopt a two-stage training strategy in which the Fourier feature parameters and the neural network weights are optimized sequentially, and incorporate adaptive loss weighting. To further enhance the approximation accuracy, a median filter is applied to the spatial data, and the predicted solution is constrained through a bounded linear mapping. Moreover, for certain nonlinear problems, we introduce a modified loss function inspired by the upwind numerical scheme to alleviate the excessive smoothing of discontinuous solutions typically observed in neural network approximations.

1 Introduction

In recent decades, artificial neural networks (ANNs) have had a significant impact on various tasks. As an important role of ANNs, these are a computational model in machine learning. Artificial neural networks are developed to be capable for solving desired problems. According to the properties of a special problem, the architecture and training process of the networks should be designed in an appropriate way.

Physics-informed neural networks (PINNs)[9] are a type of universal function approximators that can embed the knowledge of any physical laws that govern a given data-set in the learning process, and can be described by partial differential equations (PDEs). In other words PINNs are designed to be trained to satisfy the given training data as well as the imposed governing equations. The use of physical laws as regularization agents helps the neural network to learn the models in a limited space of admissible solutions. This property is advantageous especially when low data are available or even data are sparse and incomplete. Therefore, this strategy avoids the over fitted models. Automatic differentiation (AD) [1] is the main tool in PINNs that computes the required derivatives in the partial differential equations.

Physics-informed neural networks (PINNs) combine machine learning techniques with physical laws to numerically solve partial differential equations (PDEs). In this framework, a parametric neural network $\hat{u}(\mathbf{x}, t; \boldsymbol{\theta})$ is employed as an approximation to the unknown solution $u(\mathbf{x}, t)$. The network parameters $\boldsymbol{\theta}$ are trained such that the resulting approximation simultaneously satisfies the governing equation together with the prescribed initial and boundary conditions. The general problem can be formulated as

$$\mathcal{N}[u](\mathbf{x}, t) = 0, \quad \mathbf{x} \in \Omega, \quad t \in [0, T],$$

subject to the initial condition

$$u(\mathbf{x}, 0) = u_0(\mathbf{x}), \quad \mathbf{x} \in \Omega,$$

and the boundary condition

$$\mathcal{B}[u](\mathbf{x}, t) = g(\mathbf{x}, t), \quad (\mathbf{x}, t) \in \partial\Omega \times [0, T],$$

where \mathcal{N} denotes the differential operator associated with the governing equation, \mathcal{B} is the boundary operator, Ω represents the spatial domain, and T is the final time.

The training process is carried out by minimizing a composite loss function that enforces the PDE residual, the initial condition, and the boundary condition simultaneously. The collocation points associated with the PDE residual are denoted by $\{\mathbf{x}_{\text{PDE}}^i, t_{\text{PDE}}^i\}_{i=1}^{n_{\text{PDE}}}$, the points corresponding to the initial condition by $\{\mathbf{x}_{\text{IC}}^i\}_{i=1}^{n_{\text{IC}}}$, and the boundary points by $\{\mathbf{x}_{\text{BC}}^i, t_{\text{BC}}^i\}_{i=1}^{n_{\text{BC}}}$. The individual loss components are defined as

$$\begin{aligned} \mathcal{L}_{\text{PDE}}(\boldsymbol{\theta}) &= \frac{1}{n_{\text{PDE}}} \sum_{i=1}^{n_{\text{PDE}}} |\mathcal{N}[\hat{u}](\mathbf{x}_{\text{PDE}}^i, t_{\text{PDE}}^i; \boldsymbol{\theta})|^2, \\ \mathcal{L}_{\text{IC}}(\boldsymbol{\theta}) &= \frac{1}{n_{\text{IC}}} \sum_{i=1}^{n_{\text{IC}}} |\hat{u}(\mathbf{x}_{\text{IC}}^i, 0; \boldsymbol{\theta}) - u_0(\mathbf{x}_{\text{IC}}^i)|^2, \\ \mathcal{L}_{\text{BC}}(\boldsymbol{\theta}) &= \frac{1}{n_{\text{BC}}} \sum_{i=1}^{n_{\text{BC}}} |\mathcal{B}[\hat{u}](\mathbf{x}_{\text{BC}}^i, t_{\text{BC}}^i; \boldsymbol{\theta}) - g(\mathbf{x}_{\text{BC}}^i, t_{\text{BC}}^i)|^2. \end{aligned}$$

The total loss function is expressed as a weighted sum of these components,

$$\mathcal{L}(\boldsymbol{\theta}) = \lambda_{\text{PDE}} \mathcal{L}_{\text{PDE}}(\boldsymbol{\theta}) + \lambda_{\text{IC}} \mathcal{L}_{\text{IC}}(\boldsymbol{\theta}) + \lambda_{\text{BC}} \mathcal{L}_{\text{BC}}(\boldsymbol{\theta}),$$

where $\lambda_{\text{PDE}}, \lambda_{\text{IC}}, \lambda_{\text{BC}}$ are non-negative weighting coefficients.

A key advantage of PINNs is that the required derivatives are computed via automatic differentiation, eliminating the need for an explicit spatial or temporal discretization. Moreover, this framework naturally enables the integration of observational data with governing physical equations within a unified learning paradigm.

Although PINNs are efficient tools for solving PDEs, there are limitations in use of them. PINNs are unable to approximate PDEs that have strong non-linearity or sharp gradients that commonly occur in practical fluid flow problems. Some modifications are implemented on PINNs to improve efficiency of the methods. Distributed physics informed neural network (DPINN) enhances the capability of PINN by partitioning the computational domain into smaller sub-domains and installing a local PINN into smaller sub-problems [2]. Conservative PINN (cPINN) [5] is a spatial domain decomposition approach in the PINN framework tailored for conservation laws. Extended Physics informed neural network (XPINN) [6] is a generalized space-time domain decomposition to solve nonlinear partial differential equations on arbitrary complex geometry domains which pushes the boundaries of both PINNs and cPINNs.

As a drawback of neural networks, they are incapable in learning high frequencies in functions which is referred as spectral bias. In fact, they are biased towards learning low frequencies [8]. This undesired preference also prevents PINNs from learning high frequencies and fine structures of target solutions [11]. In [10] random Fourier feature is introduced to overcome the spectral bias and make the neural network capable to learn high frequencies. The Fourier feature is a powerful tool in PINNs for solving PDEs with scattered spectral solutions. A variant of this idea is used in the present work to learn solutions of PDEs with discontinuities.

Modeling discontinuous behaviors are more hard to approximate using PINNs. In its most general form, the one-dimensional advection equation can be written as

$$\frac{\partial u}{\partial t} + a(x, t, u) \frac{\partial u}{\partial x} = f(x, t, u), \quad x \in [a, b], t \geq 0, \quad (1)$$

where $u(x, t)$ denotes the advected quantity, $a(x, t, u)$ is the advection velocity, which may depend on the solution u , the spatial coordinate, and time, and $f(x, t, u)$ represents a source term. If both a and f are independent of u , the problem is linear; otherwise, it is nonlinear.

The initial condition at time $t = 0$ is prescribed as

$$u(x, 0) = u_0(x), \quad x \in [a, b].$$

Boundary conditions are imposed on the spatial boundary $\partial[a, b] = \{a, b\}$. In a compact operator form, they can be expressed as

$$\mathcal{B}[u](x, t) = g(x, t), \quad (x, t) \in \partial[a, b] \times [0, T],$$

where \mathcal{B} denotes a boundary operator consistent with the physical characteristics of the problem.

A general mixed (Robin) boundary condition is given by

$$\alpha(x, t) u(x, t) + \beta(x, t) \partial_n u(x, t) = g(x, t),$$

where α and β are prescribed coefficient functions. The Dirichlet condition corresponds to $\alpha \neq 0$ and $\beta = 0$, yielding $u = g$, whereas the Neumann condition corresponds to $\alpha = 0$ and $\beta \neq 0$, leading to $\partial_n u = g/\beta$.

In the one-dimensional setting, the outward normal derivative reduces to $\partial_n u = \pm \partial_x u$, where the sign depends on whether the boundary point is $x = a$ or $x = b$. The coefficient functions α and β , as well as the prescribed boundary data g , may depend on both space and time and may take different values at the left and right boundaries.

This equation describes the passive advection of some scalar field $u(x, t)$ carried along by a flow of speed a . This equation must surely be the simplest of all partial differential equations. Yet to approximate it well on a fixed (x, t) -mesh is a far from trivial problem that is still under active discussion in the numerical analysis literature [7]. The exact solution of this equation is constant along the characteristic curves associated to this equation. Since finding characteristic curves are complicated especially for system of hyperbolic equations, usually use of numerical methods is preferred. Some well-known numerical methods for solving this equation are upwind and Lax-Wendroff methods. In numerical methods for solving advection equation, preservation of maximum principle is an important subject. The upwind method preserves this property under the CFL condition while Lax-wendroff always does not preserve the property [4]. The problem is more complicated when the initial or boundary conditions have discontinuities which propagate along the characteristic curves in domain of the problem.

In this work, we focus on solving Problem 1 with discontinuous solutions. This paper is organized as follows: In Section 2, the random Fourier feature mapping is presented, along with a two-stage training procedure for solving a problem with discontinuous initial and boundary conditions. A modification in the weighting of the terms in the loss function is applied during the first training stage. In Section 3, median filtering and solution clamping techniques are introduced to mitigate noise resulting from the method proposed in Section 2. Section 4 presents a robust approach for loss function modification in the solution of nonlinear advection equations. Finally, a conclusion is provided in Section 5.

2 Fourier Feature Mapping and Two-Stage Training

Random Fourier features provide an effective mechanism to enhance the capability of neural networks to model rapidly oscillatory functions, local discontinuities, and high-frequency components. This technique was developed to mitigate the intrinsic spectral bias of multilayer perceptrons (MLPs) — the tendency of these models to learn low-frequency components first and to delay reconstruction of high-frequency details.

In this approach, an input vector $\mathbf{m} \in \mathbb{R}^d$ is mapped nonlinearly before being passed to the network:

$$\gamma(\mathbf{m}) = [\cos(\mathbf{B}\mathbf{m}), \sin(\mathbf{B}\mathbf{m})]^\top \in \mathbb{R}^{2D}, \quad (2)$$

where D denotes the number of sine–cosine pairs and $\mathbf{B} \in \mathbb{R}^{D \times d}$ is a matrix that encodes the frequency scales and directions applied to the input. The rows of \mathbf{B} are commonly sampled from a Gaussian distribution $\mathcal{N}(0, \sigma^2)$. For the one-dimensional advection problem considered here one may take $\mathbf{m} = [x, t]^\top$.

The parameter σ controls the frequency spectrum of the random Fourier features and thereby governs the relative contribution of low- and high-frequency components in the mapping. Increasing σ improves the network’s ability to capture oscillatory components and fine-scale variations, whereas excessively large values of σ may lead to instability, overfitting, and Gibbs-like artifacts.

Besides improving representational capacity, the Fourier feature mapping often yields faster optimizer convergence: the transformed input exposes both low- and high-frequency components to the network in a quasi-linear fashion, allowing the model to represent localized structures and discontinuities more effectively without increasing network depth or architectural complexity. In practice, achieving satisfactory performance typically requires increasing D , which raises training cost. Moreover, in the presence of discontinuities an imbalance between different loss components may still persist and remains a challenge.

2.1 Trainable Fourier Feature Mapping

Empirical evidence indicates that training the Fourier feature mapping parameters (i.e., the entries of the matrix \mathbf{B} in (2)) prior to training the neural network produces a more targeted feature transform that is beneficial for representing discontinuities. Accordingly, we propose a two-stage training scheme in which the Fourier feature mapping parameters are learned separately in the first stage. The goal is to obtain features that provide a suitable representation of the input data so that the neural network can process them effectively.

This two-stage strategy significantly accelerates training in the presence of discontinuities and helps to rebalance the contributions of different terms in the loss function. In the first stage one may use optimizers such as Adam or L-BFGS. To prevent premature stagnation during the initial training stage, particularly when employing the LBFGS optimizer, an appropriate initialization of the network parameters is crucial. In this regard, the network weights are initialized using the Glorot [3] scheme, while the bias terms are set to zero. Note that during this stage the network parameters may change only marginally; nevertheless, continuing the mapping optimization is useful because it facilitates the subsequent stage. Longer training in the first stage tends to balance the discontinuous components relative to the smooth ones, thereby expediting overall convergence. Useful stopping criteria for the mapping stage include the absolute maximum and the mean magnitude of the entries of \mathbf{B} . Once the Fourier feature mapping has stabilized, the neural network parameters are trained separately. The training data remain identical across both stages.

In other words, suppose the model is written as

$$\hat{u}(x, t; \boldsymbol{\theta}) = N(\gamma(x, t; \boldsymbol{\theta}_1); \boldsymbol{\theta}_2),$$

where $\boldsymbol{\theta}_1$ denotes the Fourier feature mapping parameters and $\boldsymbol{\theta}_2$ denotes the neural-network parameters. In the first stage $\boldsymbol{\theta}_2$ is frozen while $\boldsymbol{\theta}_1$ is optimized; subsequently $\boldsymbol{\theta}_1$ is frozen and $\boldsymbol{\theta}_2$ is optimized. This procedure enables the network to effectively exploit the learned Fourier feature mapping and improves the overall training performance. Figure 1 compares the evolution of the different loss components when random Fourier features and the two-stage training are applied to the advection problem.

$$u_t + 2u_x = 0, \quad u(0, t) = 0, \quad u(x, 0) = \begin{cases} 0.6, & |x - 0.2| \leq 0.1, \\ 0.8, & |x - 0.55| \leq 0.1, \\ 1.0, & |x - 0.9| \leq 0.1, \\ 0.8, & |x - 1.25| \leq 0.1, \\ 0.6, & |x - 1.6| \leq 0.1, \\ 0, & \text{otherwise.} \end{cases} \quad (3)$$

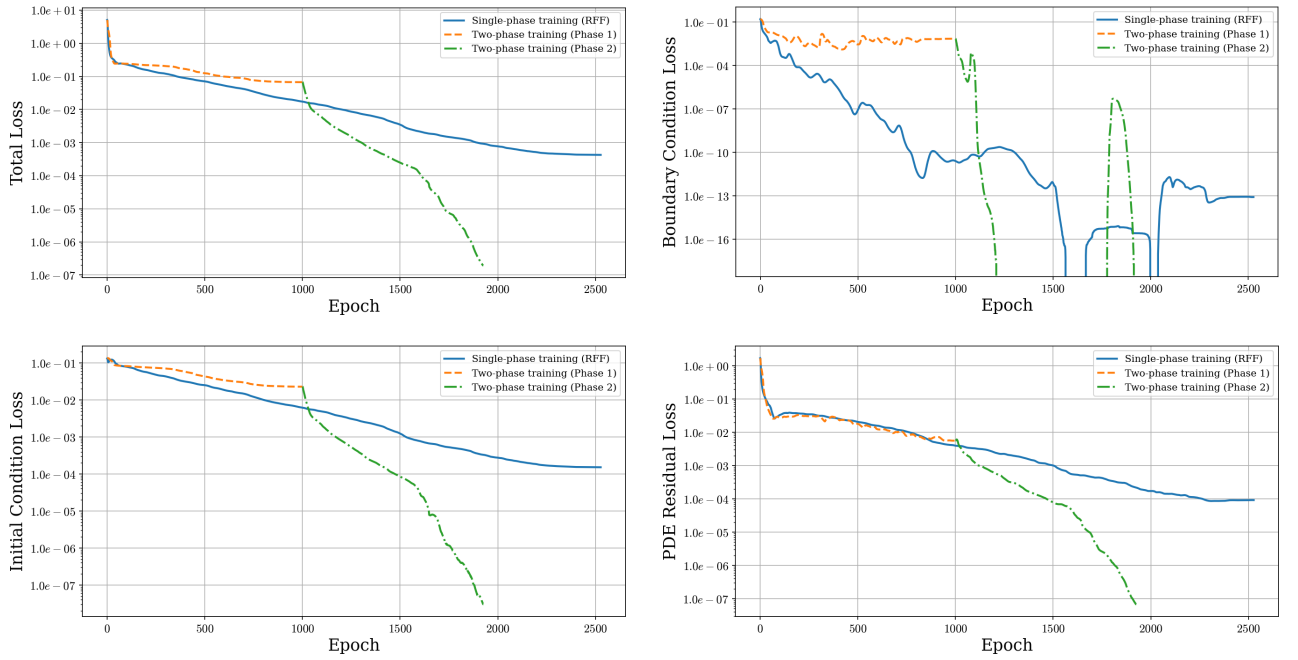


Figure 1: Evolution of the individual loss components when using random Fourier features and the two-stage training strategy.

It is clear from the results shown in Figure 1 that, after the second stage of the two-phase training, the loss function converges to zero at an accelerated rate. This behavior demonstrates the efficiency of the proposed two-phase Fourier training compared to the single-phase approach.

2.2 Adaptive Fourier Weighting

Since, in the presence of discontinuous conditions, the primary source of imbalance in the loss function is typically the discontinuity itself, we propose assigning a significantly larger weight to the loss component associated with the discontinuous part during the first training stage, i.e., the optimization of the Fourier-mapping parameters. We refer to this strategy as adaptive Fourier weighting. This weighting scheme focuses the first-stage optimization of the Fourier mapping on regions containing discontinuities and ultimately leads to faster and more balanced learning of these features in the second stage. The resulting feature space is therefore

better aligned with the specific requirements of modeling discontinuous solutions. Moreover, this adaptive adjustment reduces the likelihood of convergence to undesirable local minima and steers the training process toward improved solutions. Empirically, the training speed can improve by several factors, while alleviating the need for highly complex neural network architectures.

In the second training stage, i.e., during optimization of the neural-network parameters, one may employ alternative weighting strategies such as gradient-norm-based methods, NTK-based weighting, or any other suitable adaptive scheme. The combination of two-stage training with the proposed adaptive weighting is effective both in balancing the different components of the loss function and in substantially reducing the overall training time.

Figure 2 compares the individual loss components for the two-stage training strategy with and without adaptive Fourier weighting when solving problem 3. In the adaptive weighting applied during the first stage, the loss term corresponding to the initial condition is assigned a weight that is ten times larger than those of the remaining components. In both cases, gradient-norm-based adaptive weighting is employed during the second training stage.

Despite these advantages, the aforementioned measures may lead to excessive growth of the entries of the matrix \mathbf{B} , increasing the risk of overfitting and exacerbating Gibbs-like phenomena. Mitigation strategies for these issues are discussed in Section 3.

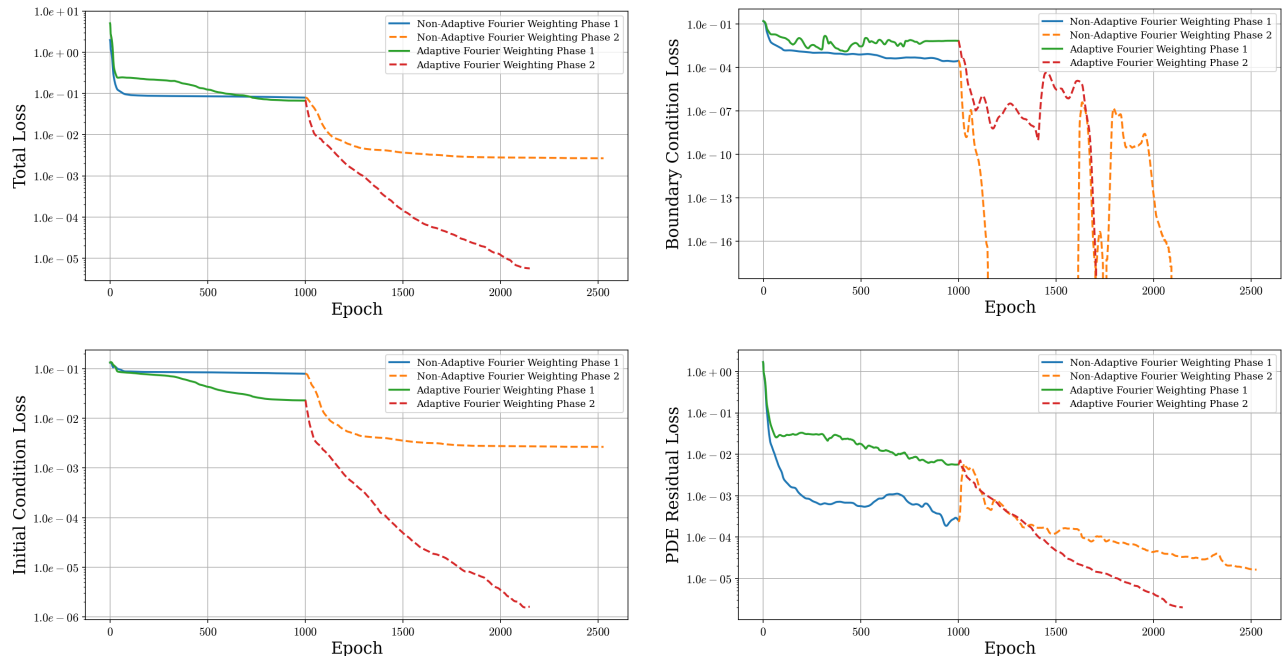


Figure 2: Comparison of the loss components for two-stage training with and without adaptive Fourier weighting applied during the optimization of the Fourier-mapping parameters.

3 Median Filtering and Bounded Approximation

Although the strategy proposed in Section 2 can significantly accelerate training and facilitate the optimization process, the increased frequency content of the Fourier mapping—equivalently, the growth of the entries of the matrix \mathbf{B} in (2)—may lead to overfitting and Gibbs-like phenomena. In such cases, the error exhibits sharp, impulse-like behavior resembling shock artifacts. In the following, we present two remedies to mitigate these issues.

3.1 Median Filtering

Median filtering smooths data by replacing each value with the median of its neighboring values. Compared to other smoothing techniques such as mean filtering, the median filter is more robust to impulsive noise and, importantly, preserves discontinuities.

Given a sorted data vector

$$\mathbf{x} = [x_1, x_2, \dots, x_N],$$

the median filter with a window of length k (an odd integer) is defined such that the filtered value at index i is

$$x_i^{(\text{filtered})} = \mathcal{M}(x_{i-m}, \dots, x_i, \dots, x_{i+m}), \quad m = \frac{k-1}{2},$$

where x_i denotes the original data at location i , k is the window size, and \mathcal{M} denotes the median operator over the interval $[i-m, i+m]$.

Our investigations indicate that applying the median filter directly to spatio-temporal data or purely temporal data may introduce large and nonphysical distortions. Therefore, we recommend computing the solution independently at each time instance and applying the median filter exclusively to the spatial data. This strategy effectively avoids the aforementioned artifacts.

Specifically, at spatial points x_i equally spaced with distance h , the filtered solution is given by

$$\hat{u}(x, t) = \mathcal{M}(N(x - mh, t; \boldsymbol{\theta}), \dots, N(x, t; \boldsymbol{\theta}), \dots, N(x + mh, t; \boldsymbol{\theta})), \quad m = \frac{k-1}{2}.$$

The parameters h and k are selected based on the problem setting. Larger values of k and h correspond to a wider neighborhood involved in the filtering process. Moreover, it is recommended to avoid applying the filter near domain boundaries.

Figures 3 and 4 present selected snapshots corresponding to some of the most challenging time instances for the solution of the advection equation

$$u_t + 2u_x = 0, \quad x \in [0, 2], \quad t \in [0, 1],$$

with the initial and boundary conditions

$$u(0, t) = \begin{cases} 0.5, & t \geq 0.5, \\ 0, & \text{otherwise,} \end{cases} \quad u(x, 0) = \begin{cases} 0.6, & |x - 0.2| \leq 0.1, \\ 0.8, & |x - 0.55| \leq 0.1, \\ 1.0, & |x - 0.9| \leq 0.1, \\ 0.8, & |x - 1.25| \leq 0.1, \\ 0.6, & |x - 1.6| \leq 0.1, \\ 0, & \text{otherwise.} \end{cases}$$

The results correspond to twenty independent training runs using a limited number of interior collocation points. Furthermore, the Fourier parameters were allowed to grow without regularization in order to increase the likelihood of noise contamination and reduce generalization capability. A simpler neural network architecture than usual was also employed. Despite these deliberately unfavorable conditions, applying the median filter to the spatial data effectively eliminates the spurious oscillations.

It is worth noting that such noise patterns are often unavoidable in practice, even when careful training strategies are adopted. In the above experiment, the mean absolute error averaged over twenty runs at the test points was 0.0046685 for the unfiltered solution, 0.0042665

for the filtered solution, and 0.0041907 for the filtered solution excluding boundary regions. This highlights that, while the raw network output may exhibit suboptimal performance on test data, the filtered solution can provide a substantially improved approximation.

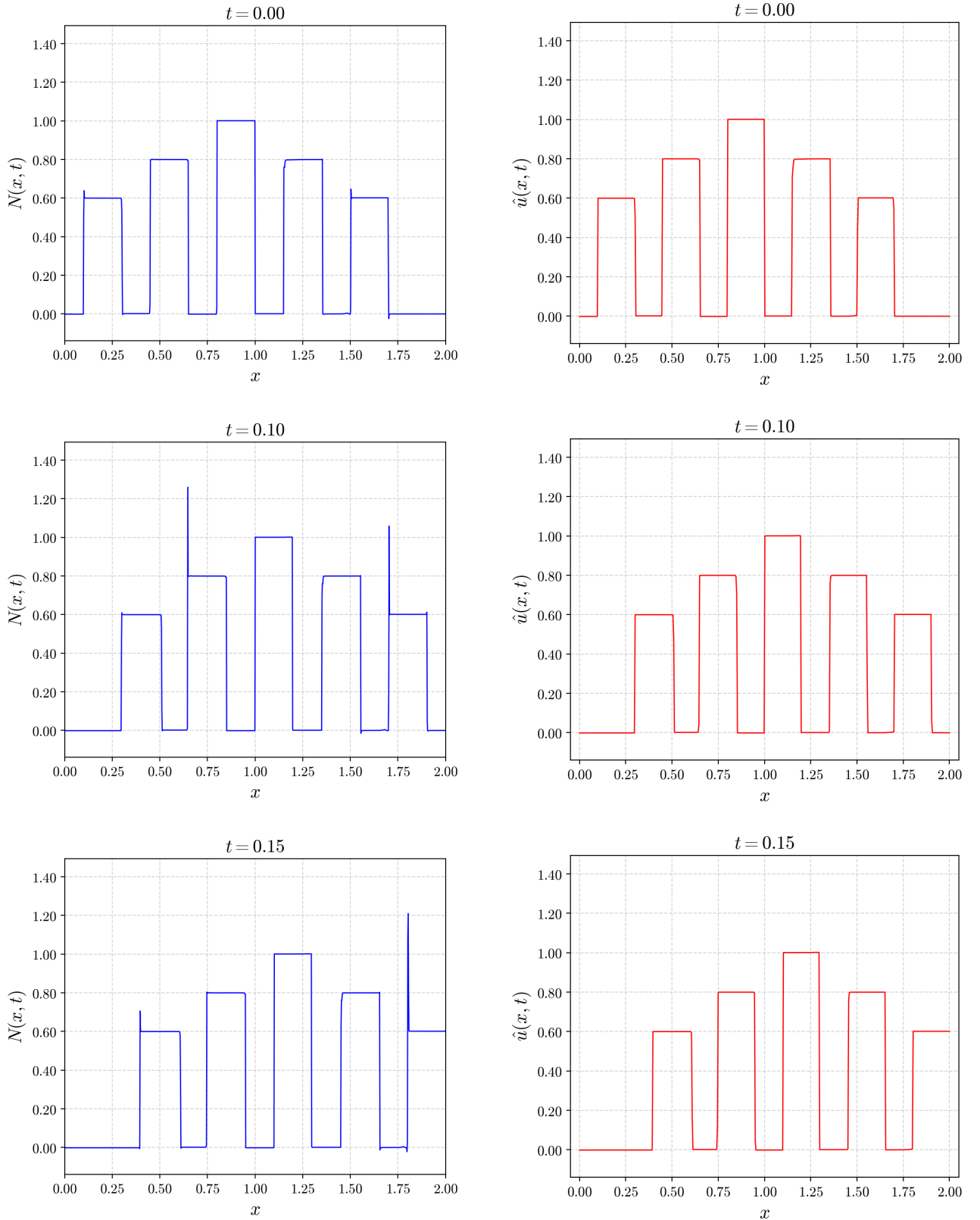


Figure 3: Filtered and unfiltered solutions at times $t = 0, 0.1$, and 0.15 .

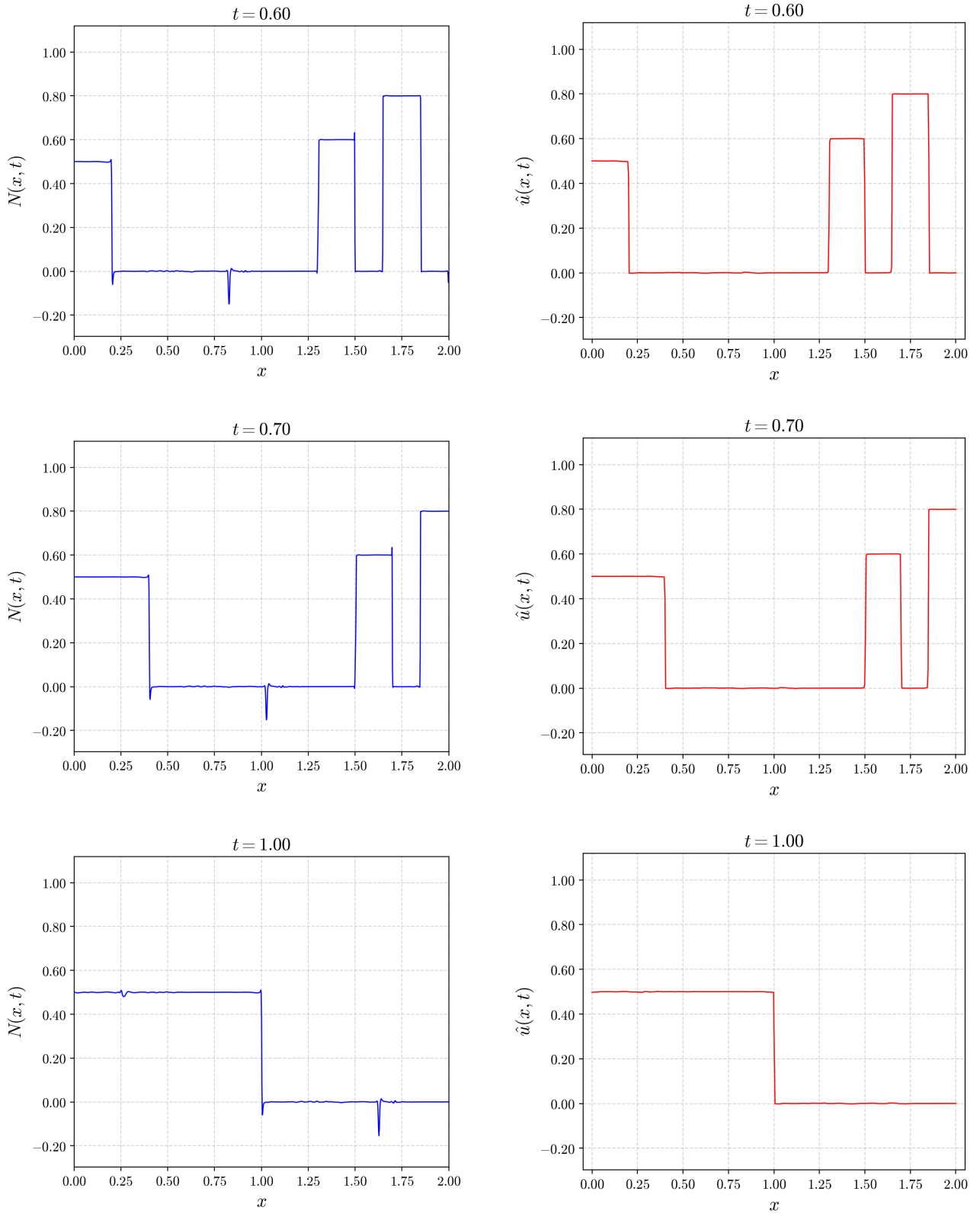


Figure 4: Filtered and unfiltered solutions at times $t = 0.6, 0.7$, and 1 .

As long as the observed oscillations do not correspond to genuine features of the true solution, the proposed filtering strategy remains effective. Allowing excessive growth of the Fourier parameters accelerates and balances the loss reduction, albeit at the cost of increased approximation error. However, since the structure of the induced error is known, median filtering can successfully remove these artifacts. Provided that the filtered solution does not exhibit sharp, narrow error spikes, the overall approximation quality remains satisfactory.

Nevertheless, while median filtering often improves solution quality, it may degrade accuracy when the true solution itself contains sharp physical features. In such cases, these locations can sometimes be identified, and the median filter may be selectively disabled in their vicinity.

3.2 Bounding the Approximate Solution

In many cases, particularly for homogeneous advection equations, the maximum and minimum values of the exact solution are known *a priori*. In such situations, it is advantageous to explicitly constrain the neural network approximation within these bounds by imposing a hard constraint on the output. Let M and m denote the maximum and minimum values of the solution, respectively. The bounded approximation is then defined as

$$\hat{u}(x, t; \boldsymbol{\theta}) = \frac{1}{2}[(M - m) \sin(N(x, t; \boldsymbol{\theta})) + M + m].$$

In the presence of discontinuities, this strategy is particularly effective, as it prevents the emergence of large spurious oscillations and unbounded approximation errors. By restricting the range of the neural network output, the model is forced to respect the physical bounds of the solution, which significantly stabilizes the learning process near discontinuities.

Figure 5 provides a schematic overview of the proposed framework, summarizing the techniques introduced in Sections 2 and 3.

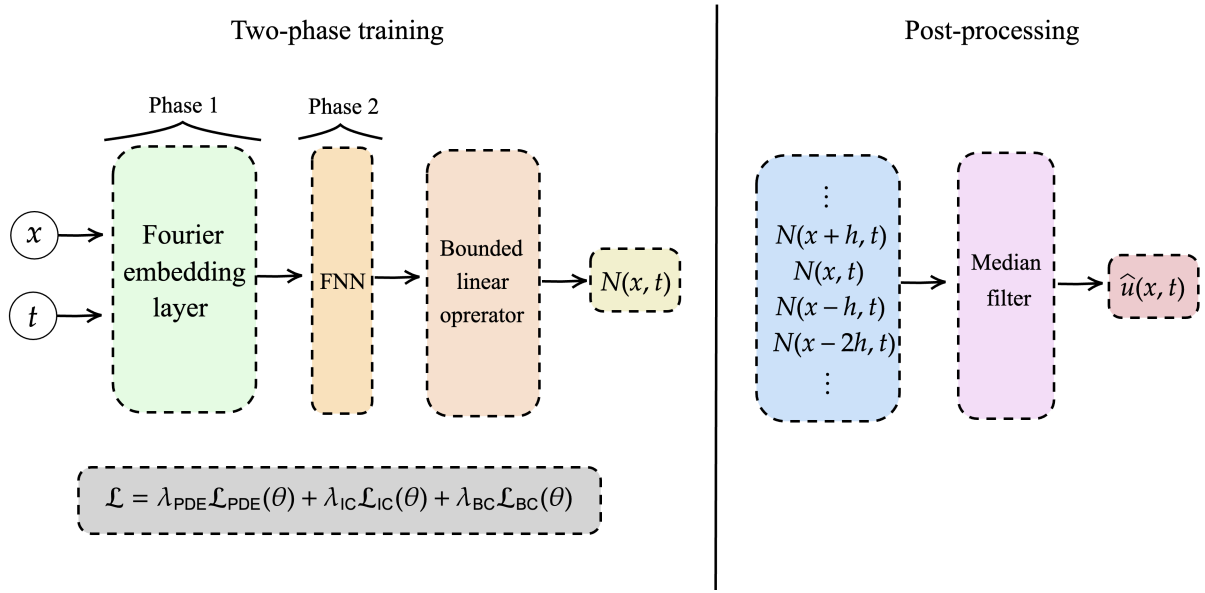


Figure 5: Schematic diagram of the proposed method

Figure 6 illustrates the approximate solution of the advection equation

$$u_t + 0.6 \sin(6xt) u_x = 0, \quad x \in [0, 2], \quad t \in [0, 1],$$

subject to the initial and boundary conditions

$$u(0, t) = 0, \quad u(x, 0) = \begin{cases} 0.6, & |x - 0.2| \leq 0.1, \\ 0.8, & |x - 0.55| \leq 0.1, \\ 1, & |x - 0.9| \leq 0.1, \\ 0.8, & |x - 1.25| \leq 0.1, \\ 0.6, & |x - 1.6| \leq 0.1, \\ 0, & \text{otherwise.} \end{cases}$$

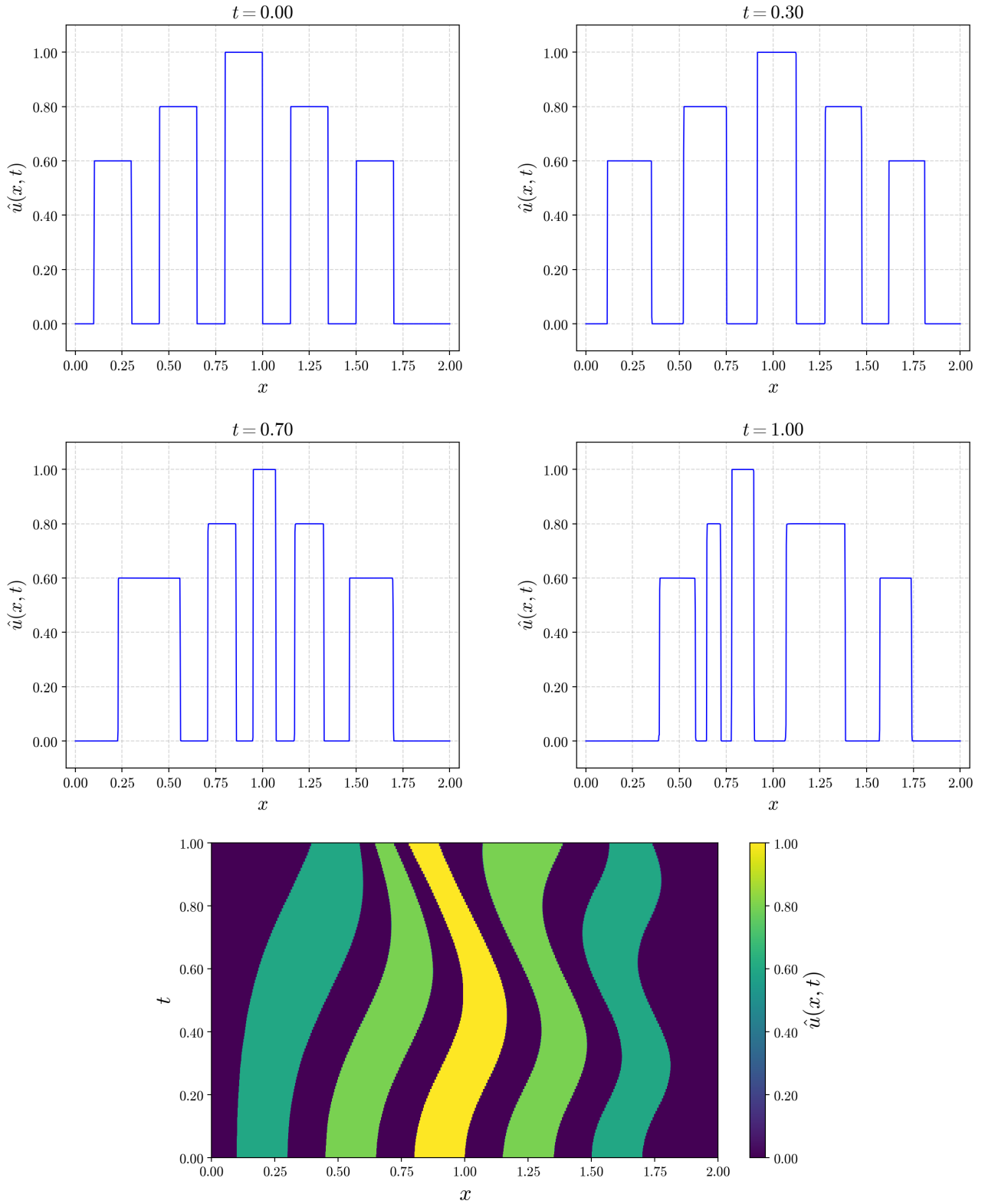


Figure 6: Approximate solution of the transport equation $u_t + 0.6 \sin(6xt) u_x = 0$.

4 Upwind Loss Function

When approximating discontinuous functions, neural networks—due to their inherently continuous nature—approximate the discontinuous behavior by steep but continuous transitions within a small neighborhood around the discontinuity point that contains training data. The slope of this transition depends on the training data distribution: the smaller the radius of

this neighborhood, the steeper the slope and the more accurate the approximation. Such an approximation is often harmless in numerical computations; however, in some cases it can become problematic.

As discussed earlier, when solving advection equations with discontinuous initial or boundary conditions, the continuous function \hat{u} assumes different values within a neighborhood I of a discontinuity point due to continuity. If the coefficient function a in equation (1) depends on u , then the propagation speed of the solution over the interval I takes significantly different values. This leads to different propagation speeds for points within the interval I , and as time evolves, it results in a noticeable discrepancy between the approximate solution and the exact solution of the problem. Although increasing the number of points associated with the initial and boundary conditions can reduce the size of the interval of interest, this significantly slows down the training process and does not fundamentally eliminate the issue.

Consider the equation

$$u_t + u(1-x)(1.5+t)u_x = 0,$$

with initial and boundary conditions

$$u(0, t) = 0, \quad u(x, 0) = \begin{cases} 1, & |x - 1| \leq 0.1, \\ 0, & \text{otherwise,} \end{cases} \quad x \in [0, 2], \quad t \in [0, 1].$$

For this problem, the loss function $\mathcal{L}_{\text{PDE}}(\theta)$ is defined as

$$\frac{1}{n_{\text{PDE}}} \sum_{i=1}^n \left| \frac{\partial \hat{u}}{\partial t}(x_{\text{PDE}}^i, t_{\text{PDE}}^i; \theta) + \hat{u}(x_{\text{PDE}}^i, t_{\text{PDE}}^i)(1 - x_{\text{PDE}}^i)(1.5 + t_{\text{PDE}}^i) \frac{\partial \hat{u}}{\partial x}(x_{\text{PDE}}^i, t_{\text{PDE}}^i; \theta) \right|^2.$$

Figure 7 illustrates the approximate solution obtained using this loss. Clearly, the solution of the advection equation in this example takes only the values zero and one. However, due to the approximation of the discontinuous initial condition by a continuous function, \hat{u} takes all values between zero and one. The u -dependent propagation speed in different regions causes some parts of the solution to lag behind others. To resolve this issue, we introduce a slight modification to the objective function.

As is known, in this example we always have $u \geq 0$, and therefore the coefficient of u_x is always nonnegative. Define $\hat{v}(x, t) = \hat{u}(x + h, t)$ where $h > 0$ is a small constant. We then define the modified loss $\tilde{\mathcal{L}}_{\text{PDE}}(\theta)$ as

$$\frac{1}{n_{\text{PDE}}} \sum_{i=1}^n \left| \frac{\partial \hat{u}}{\partial t}(x_{\text{PDE}}^i, t_{\text{PDE}}^i; \theta) + \max\{\hat{u}_i, \hat{v}_i\}(1 - x_{\text{PDE}}^i)(1.5 + t_{\text{PDE}}^i) \frac{\partial \hat{u}}{\partial x}(x_{\text{PDE}}^i, t_{\text{PDE}}^i; \theta) \right|^2,$$

where $u_i = u(x_{\text{PDE}}^i, t_{\text{PDE}}^i)$ and $v_i = v(x_{\text{PDE}}^i, t_{\text{PDE}}^i)$.

This modification of the loss function prevents the lagging of certain points relative to others when encountering a discontinuity. In fact, at each collocation point (x_i, t_i) , $i = 1, \dots, n_{\text{PDE}}$, the propagation speed is determined by the maximum of

$$\hat{u}(x_i, t_i)(1 - x_i)(1.5 + t_i) \quad \text{and} \quad \hat{u}(x_i + h, t_i)(1 - x_i)(1.5 + t_i),$$

which results in approximately uniform propagation speed for all points in the neighborhood of the discontinuity. Clearly, the more training data located in a smaller neighborhood around the discontinuity, the smaller value of h can be chosen.

Since $|\max\{b, c\} - b| \leq |c - b|$, by the mean value theorem we have

$$|\max\{u(x, t), u(x + h, t)\} - u(x, t)| \leq |u(x + h, t) - u(x, t)| = h \frac{\partial u}{\partial x}(\xi, t), \quad \xi \in [x, x + h].$$

Therefore, points whose spatial derivatives are controlled within a neighborhood of length h , such a modification does not significantly alter the solution.

We further propose to approximate the max function as

$$\max\{b, c\} \approx \sigma(\alpha(b - c))b + \sigma(-\alpha(b - c))c, \quad (4)$$

where σ denotes the sigmoid function, $\sigma(x) = 1/(1 + e^{-x})$. This approximation is stable for sufficiently large values of α and provides a good approximation when b and c are close to each other; it is exact when $b = c$. In contrast, other approximations of the max function, such as the log-sum-exp (LSE), may lead to instability and inaccuracies when the arguments are close.

The approximate solution obtained using the modified objective function is shown in Figure 8. Although this example exploits the sign of the solution and the direction of propagation, we now present a more general and comprehensive approach that does not rely on prior knowledge of the solution.

Suppose the objective is to solve

$$u_t + u a(x, t)u_x = f(x, t, u).$$

Define $\hat{v} = \hat{u}(x + h, t)$ and $\hat{w} = \hat{u}(x - h, t)$, and define the modified loss $\tilde{\mathcal{L}}_{\text{PDE}}(\theta)$ as

$$\frac{1}{n_{\text{PDE}}} \sum_{i=1}^n \left| \frac{\partial \hat{u}}{\partial t}(x_{\text{PDE}}^i, t_{\text{PDE}}^i; \theta) + r(\hat{v}_i, \hat{w}_i) a(x_{\text{PDE}}^i, t_{\text{PDE}}^i) \frac{\partial \hat{u}}{\partial x}(x_{\text{PDE}}^i, t_{\text{PDE}}^i; \theta) - f_i \right|^2,$$

where

$$r(b, c) = \begin{cases} b, & |b| \geq |c|, \\ c, & |c| > |b|, \end{cases} \quad (5)$$

and

$$f_i = f(x_{\text{PDE}}^i, t_{\text{PDE}}^i, u(x_{\text{PDE}}^i, t_{\text{PDE}}^i)).$$

Thus, at each collocation point, the propagation speed is replaced by the value with the larger absolute magnitude among the neighboring points. By the mean value theorem, we obtain

$$|r(u(x - h, t), u(x + h, t)) - u(x, t)| = h \frac{\partial u}{\partial x}(\xi, t), \quad \xi \in [x - h, x + h]. \quad (6)$$

Define

$$\ell_{\text{PDE}}(\theta) = \max_i \left| \frac{\partial \hat{u}}{\partial t}(x_{\text{PDE}}^i, t_{\text{PDE}}^i; \theta) + \hat{u}(x_{\text{PDE}}^i, t_{\text{PDE}}^i) a(x_{\text{PDE}}^i, t_{\text{PDE}}^i) \frac{\partial \hat{u}}{\partial x}(x_{\text{PDE}}^i, t_{\text{PDE}}^i; \theta) - f_i \right|,$$

and

$$\tilde{\ell}_{\text{PDE}}(\theta) = \max_i \left| \frac{\partial \hat{u}}{\partial t}(x_{\text{PDE}}^i, t_{\text{PDE}}^i; \theta) + r(\hat{v}_i, \hat{w}_i) a(x_{\text{PDE}}^i, t_{\text{PDE}}^i) \frac{\partial \hat{u}}{\partial x}(x_{\text{PDE}}^i, t_{\text{PDE}}^i; \theta) - f_i \right|.$$

Using (6), we obtain

$$\begin{aligned} \ell_{\text{PDE}}(\theta) - \tilde{\ell}_{\text{PDE}}(\theta) &\leq |\ell_{\text{PDE}}(\theta) - \tilde{\ell}_{\text{PDE}}(\theta)| \\ &\leq \max_i \left| h \frac{\partial u}{\partial x}(\xi_i, t_{\text{PDE}}^i; \theta) a(x_{\text{PDE}}^i, t_{\text{PDE}}^i) \frac{\partial \hat{u}}{\partial x}(x_{\text{PDE}}^i, t_{\text{PDE}}^i; \theta) \right| \\ &\leq h \max_i |a(x_{\text{PDE}}^i, t_{\text{PDE}}^i) M_i^2|, \end{aligned} \quad (7)$$

where

$$\xi_i \in I_i = [x_{\text{PDE}}^i - h, x_{\text{PDE}}^i + h], \quad M_i = \max_{d_i \in I_i} \left| \frac{\partial \hat{u}}{\partial x}(d_i, t_{\text{PDE}}^i; \theta) \right|.$$

Consequently,

$$\mathcal{L}_{\text{PDE}}(\theta) \leq [\ell_{\text{PDE}}(\theta)]^2 \leq \left[\tilde{\ell}_{\text{PDE}}(\theta) + h \max_i |a(x_{\text{PDE}}^i, t_{\text{PDE}}^i) M_i^2| \right]^2.$$

Assuming $\ell_{\text{PDE}}(\theta)$ is small, the value of \mathcal{L}_{PDE} depends on M_i and h . For points with controlled spatial derivatives within a neighborhood of length h , the difference between \mathcal{L}_{PDE} and $\tilde{\mathcal{L}}_{\text{PDE}}$ is small. In regions where M_i is large due to a discontinuity, this discrepancy is not problematic. In fact, this modification treats steep continuous transitions similarly to discontinuities, and as long as such steep transitions are absent in the exact solution, the resulting approximation remains reliable.

We propose approximating the function r , defined in (5) as

$$r(b, c) \approx \text{Sr}(b, c) = \sigma(\alpha(\text{SA}(b) - \text{SA}(c)))b + \sigma(-\alpha(\text{SA}(b) - \text{SA}(c)))c, \quad (8)$$

where SA is a smooth approximation of the absolute value defined as

$$|b| = \max\{b, -b\} \approx \text{SA}(b) = \sigma(2\alpha b)b - \sigma(-2\alpha b)b.$$

As an example, we consider solving

$$u_t + u(0.4 - x)(1 - x)(1.6 - x)(1.5 + t) = 0, \quad x \in [0, 2], \quad t \in [0, 1],$$

with initial and boundary conditions

$$u(0, t) = 0, \quad u(x, 0) = \begin{cases} 1, & |x - 0.4| \leq 0.1, \\ -\sin\left(\frac{(x - 0.8)\pi}{0.4}\right), & |x - 1| \leq 0.2, \\ 1, & |x - 1.6| \leq 0.1, \\ 0, & \text{otherwise.} \end{cases}$$

The approximate solutions obtained using the standard and modified objective functions can be observed in Figures 9 and 10, respectively.

This modification of the loss function can be generalized to solve any equation of the form

$$u_t + a(x, t, u)u_x = f(x, t, u)$$

by defining $\tilde{\mathcal{L}}_{\text{PDE}}(\theta)$ as

$$\frac{1}{n_{\text{PDE}}} \sum_{i=0}^n \left| \frac{\partial \hat{u}}{\partial t}(x_{\text{PDE}}^i, t_{\text{PDE}}^i; \theta) + r(a(x_{\text{PDE}}^i, t_{\text{PDE}}^i, \hat{v}_i), a(x_{\text{PDE}}^i, t_{\text{PDE}}^i, \hat{w}_i)) \frac{\partial \hat{u}}{\partial x}(x_{\text{PDE}}^i, t_{\text{PDE}}^i; \theta) - f_i \right|^2.$$

Using an argument similar to (7), one can show that

$$\mathcal{L}_{\text{PDE}}(\theta) \leq \left[\tilde{\ell}_{\text{PDE}}(\theta) + \max_i \left| h \frac{\partial \hat{u}}{\partial x}(\xi_i, t_{\text{PDE}}^i; \theta) \frac{\partial a}{\partial \hat{u}}(x_{\text{PDE}}^i, t_{\text{PDE}}^i, \hat{u}(\xi_i, t_{\text{PDE}}^i; \theta)) \frac{\partial \hat{u}}{\partial x}(x_{\text{PDE}}^i, t_{\text{PDE}}^i; \theta) \right| \right]^2,$$

which demonstrates the effectiveness of the modified objective function. Note that instead of using r , the smooth approximation introduced in (8) is employed in the objective function.

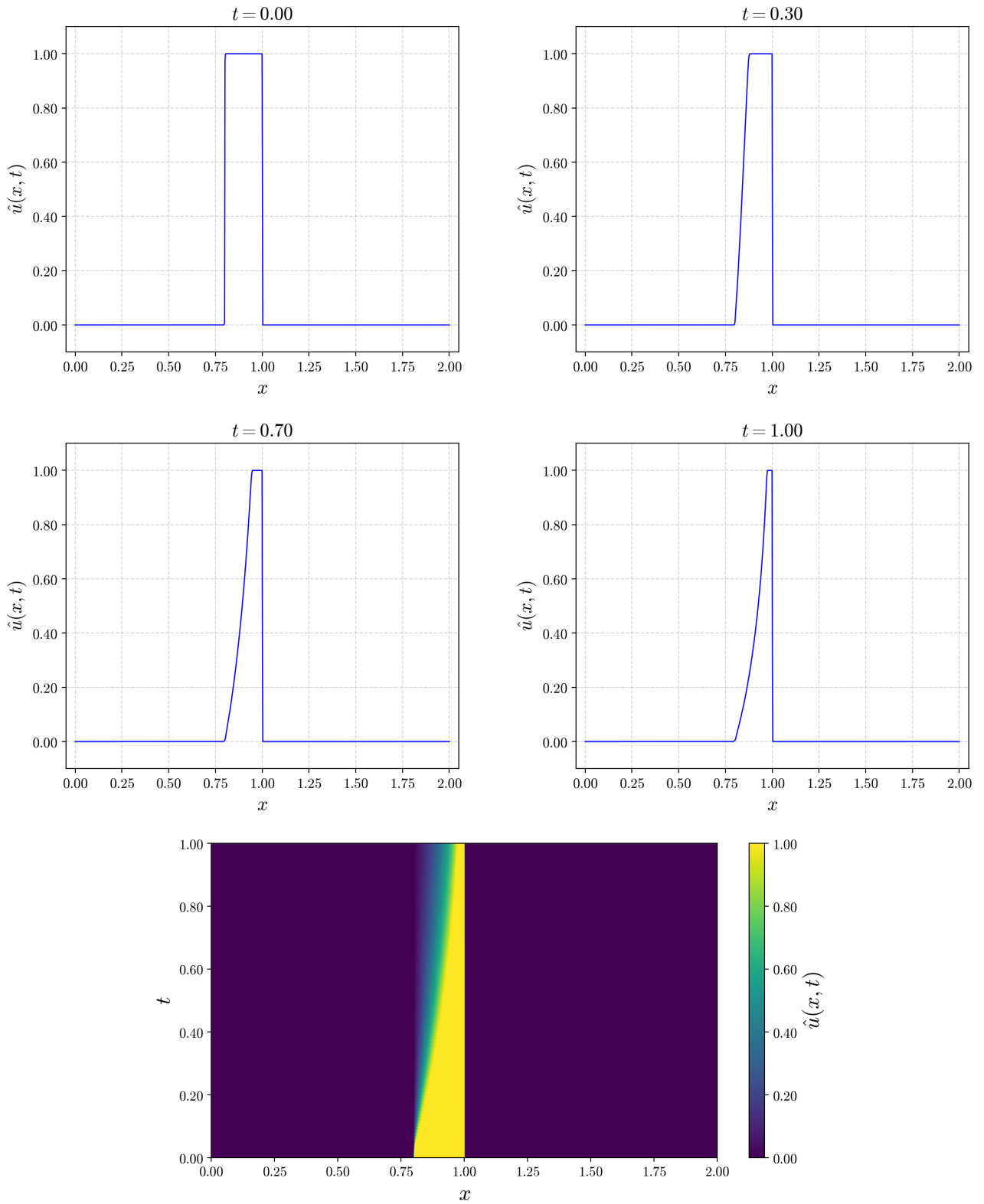


Figure 7: Solution of the advection equation $u_t + u(1-x)(1.5+t)u_x = 0$ obtained using the standard loss function.

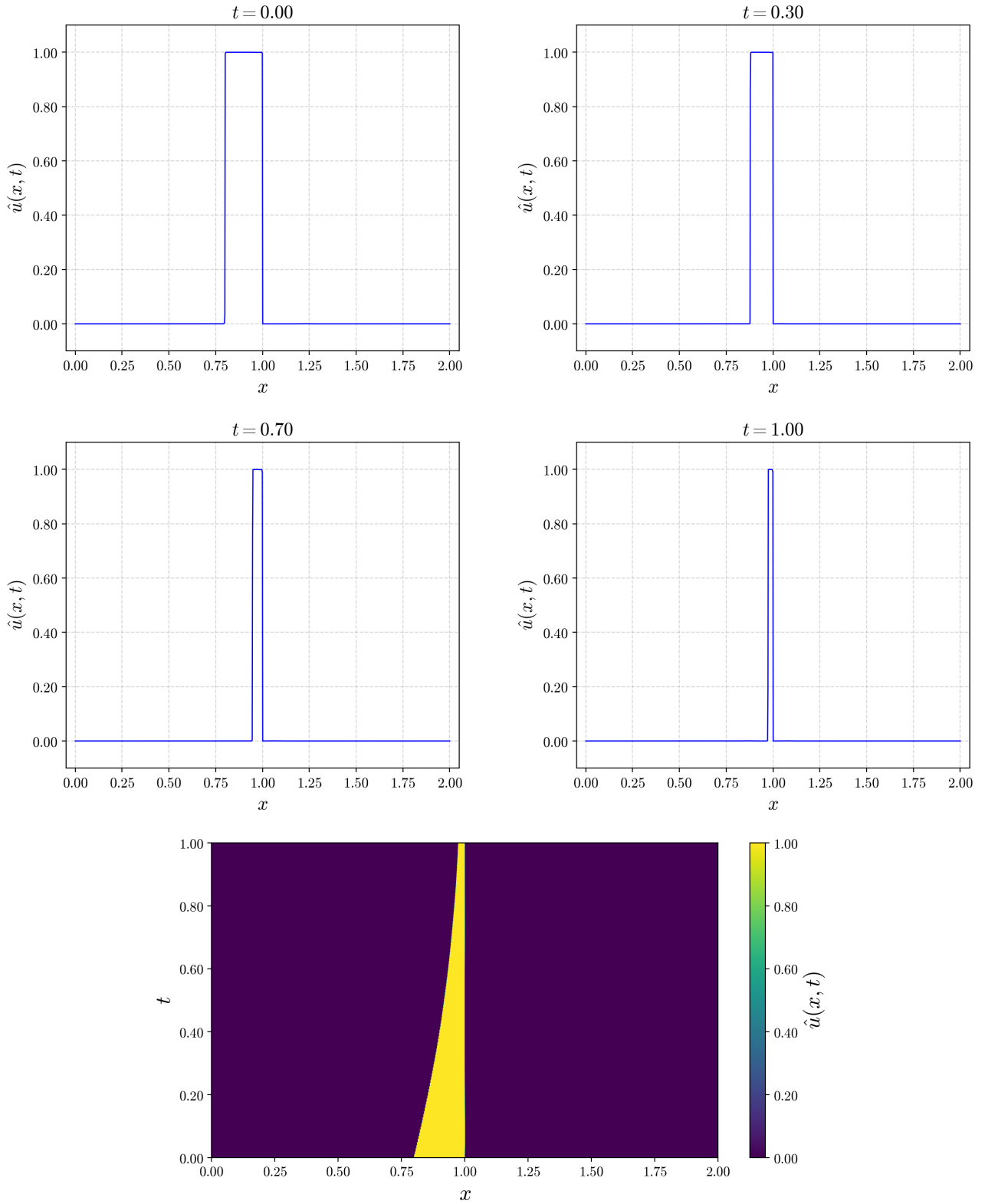


Figure 8: Solution of the advection equation $u_t + u(1-x)(1.5+t)u_x = 0$ obtained using the modified upwind loss function with $\alpha = 100$, $h = 0.01$ and 10,000 collocation points.

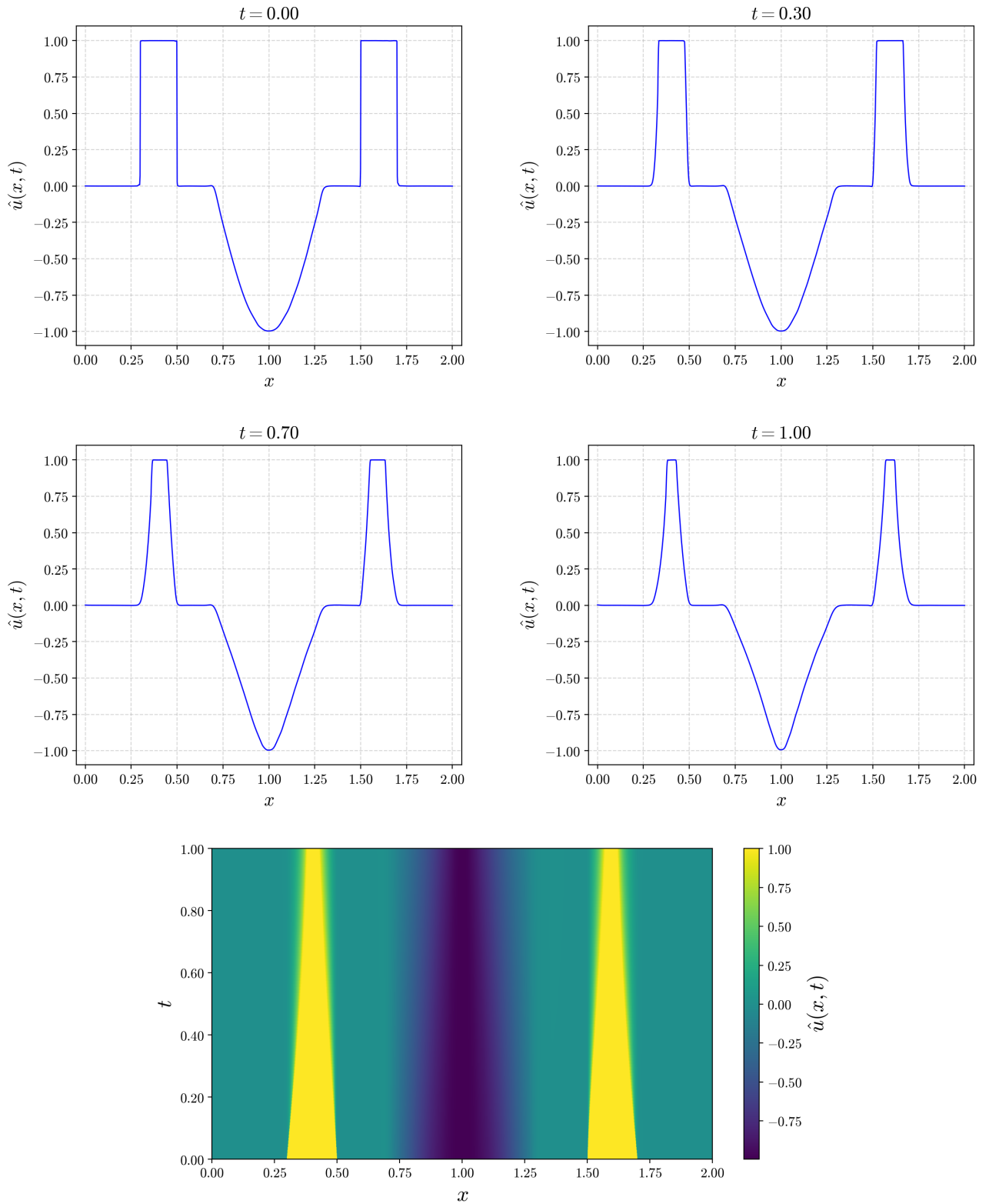


Figure 9: Solution of the advection equation $u_t + u(0.4 - x)(1 - x)(1.6 - x)(1.5 + t) = 0$ obtained using the standard loss function.

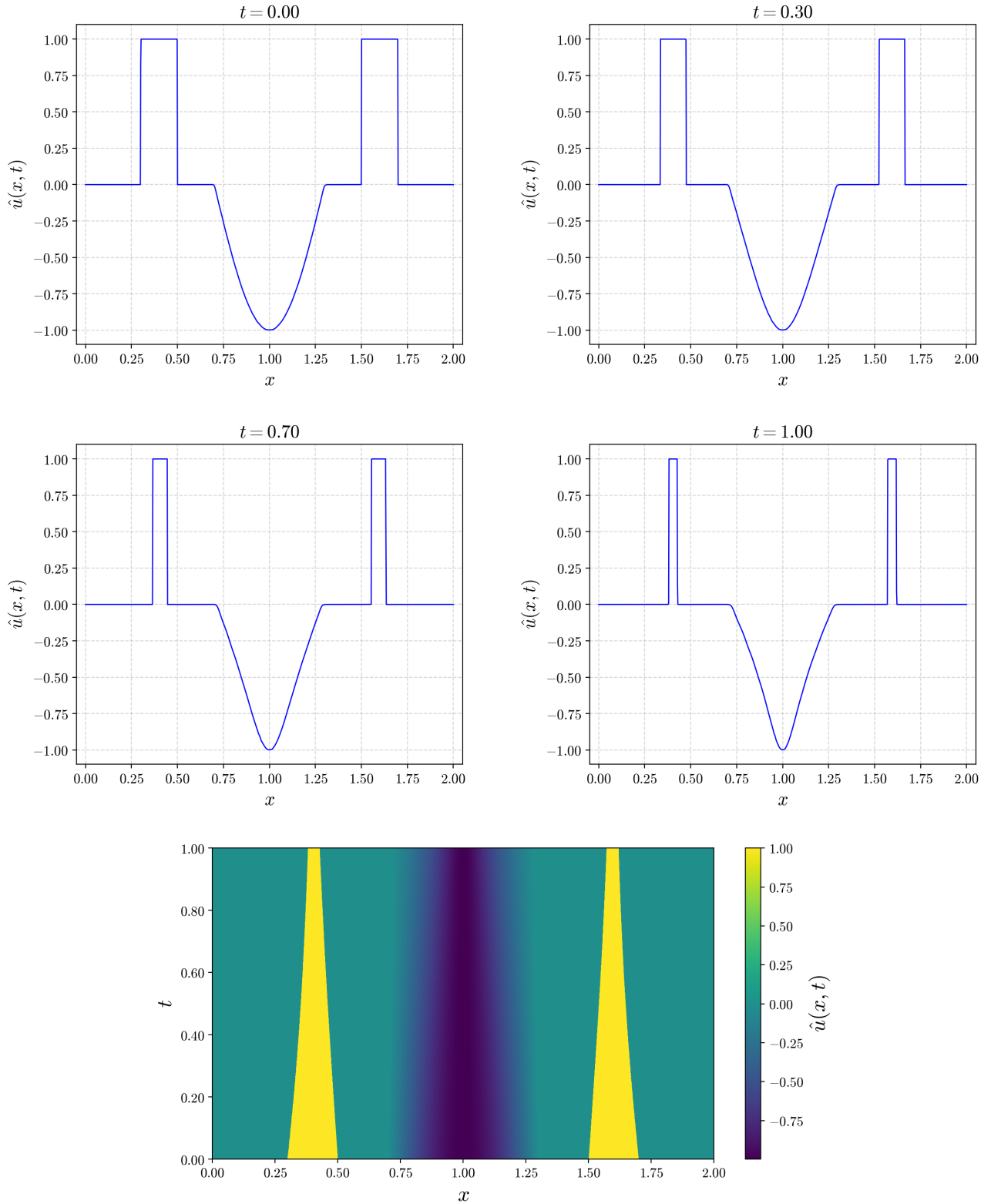


Figure 10: Solution of the advection equation $u_t + u(0.4 - x)(1 - x)(1.6 - x)(1.5 + t) = 0$ obtained using the modified upwind loss function with $\alpha = 100$, $h = 0.01$ and 10,000 collocation points.

5 Conclusion

in this study, the solution of the advection equation is investigated using Physics-Informed Neural Networks (PINNs). Considering the high computational cost of the classical PINN

approach for simulating discontinuous solutions of this equation, reducing computational expense while accurately capturing discontinuities becomes particularly important. This paper proposes strategies to overcome these challenges.

Random Fourier feature mapping provides an effective approach to mitigate the spectral bias inherent in neural networks. Here, a two-stage training scheme is proposed to efficiently and accurately simulate the discontinuities in the solution of the advection equation. In the first stage, the parameters of the Fourier feature mapping are trained, while in the second stage, the neural network parameters are optimized. The features obtained from the Fourier feature mapping in the first stage provide a more suitable representation of the training data, yielding improved performance compared to standard random Fourier features. Finally, an adaptive weighting strategy for the loss function is introduced to stabilize the training process. The results demonstrate a significant acceleration in convergence, although this may lead to overfitting, spurious spikes, and Gibbs-like phenomena in the approximate solution.

Subsequently, to suppress the noise introduced during training, a median filter is applied to the spatial data at each time step. To enhance the filter's performance, it is not applied at boundary points. Additionally, by utilizing knowledge of the solution's extrema, applying mappings to constrain the solution as a hard constraint further aids in noise reduction.

In solving nonlinear advection problems, due to the dependence of the advection coefficient on the solution itself, the approximate solution is represented as a continuous function with steep gradients at discontinuity points. This phenomenon arises from the inherent continuous nature of neural network architectures, which causes the network's output to undergo significant temporal variations. To address this challenge, a modified loss function based on a bias-aware approach using nested sigmoid approximations has been employed. This strategy enables accurate and stable approximation of the solution. The provided examples demonstrate the effectiveness of this technique.

References

- [1] A. G. Baydin, B. A. Pearlmutter, A. A. Radul, and J. M. Siskind. Automatic differentiation in machine learning: a survey. *Journal of Machine Learning Research*, 18(153):1–43, 2018.
- [2] V. Dwivedi, N. Parashar, and B. Srinivasan. Distributed learning machines for solving forward and inverse problems in partial differential equations. *Neurocomputing*, 420:299–316, 2021.
- [3] X. Glorot and Y. Bengio. Understanding the difficulty of training deep feedforward neural networks. In *Proceedings of the Thirteenth International Conference on Artificial Intelligence and Statistics*, volume 9 of *Proceedings of Machine Learning Research*, pages 249–256, Sardinia, Italy, 2010.
- [4] R. Hosseini and M. Tatari. Some splitting methods for hyperbolic PDEs. *Applied Numerical Mathematics*, 146:361–378, 2019.
- [5] A. D. Jagtap, E. Kharazmi, and G. E. Karniadakis. Conservative physics-informed neural networks on discrete domains: Applications to forward and inverse problems. *Computer Methods in Applied Mechanics and Engineering*, 365:113028, 2020.
- [6] A. D. Jagtap and G. E. Karniadakis. Extended physics-informed neural networks (XPINNs): A generalized space–time domain decomposition based deep learning framework for nonlinear partial differential equations. *Communications in Computational Physics*, 28(5):2002–2041, 2020.

- [7] K. W. Morton and D. F. Mayers. Numerical Solution of Partial Differential Equations, 2nd edition. Cambridge University Press, 2005.
- [8] N. Rahaman, A. Baratin, D. Arpit, F. Draxler, M. Lin, F. Hamprecht, Y. Bengio, and A. Courville. On the spectral bias of neural networks. In Proceedings of the International Conference on Machine Learning, pages 5301–5310, 2019.
- [9] M. Raissi, P. Perdikaris, and G. E. Karniadakis. Physics-informed neural networks: A deep learning framework for solving forward and inverse problems involving nonlinear partial differential equations. *Journal of Computational Physics*, 378:686–707, 2019.
- [10] M. Tancik, P. P. Srinivasan, B. Mildenhall, S. Fridovich-Keil, N. Raghavan, U. Singhal, R. Ramamoorthi, J. T. Barron, and R. Ng. Fourier features let networks learn high frequency functions in low dimensional domains. In *Advances in Neural Information Processing Systems*, 2020.
- [11] S. Wang, H. Wang, and P. Perdikaris. On the eigenvector bias of Fourier feature networks: From regression to solving multi-scale PDEs with physics-informed neural networks. *Computer Methods in Applied Mechanics and Engineering*, 384:113938, 2021.